BEARING CAPACITY OF NONHOMOGENEOUS CLAY LAYERS UNDER EMBANKMENTS

By Radoslaw L. Michalowski,[1] Member, ASCE, and Lei Shi,[2] Student Member, ASCE

ABSTRACT: The slip-line method is used to calculate limit loads on layers of weak soil. A horizontal load component of arbitrary intensity is accounted for. The soil is considered cohesive, with the undrained shear strength increasing with depth. The slip-line solutions presented are proved to be lower bounds to the true limit loads. The upper-bound results are also presented, though the details of the solution are omitted. Limit loads are presented in the form of graphs. The total load on the foundation soil from embankments is vertical and equal to the weight of the embankment fill. The outward-acting symmetrical tangential load under unreinforced embankments is caused, however, by the horizontal thrust in the embankment fill. A simple method for calculating this horizontal load is suggested, and a proposal for arriving at failure heights of both unreinforced and reinforced embankments is given. A failure height calculation for a case history is presented. Also, a generic example of critcal height prediction for a reinforced and an unreinforced embankment is shown.

INTRODUCTION

The bearing capacity of layers has been addressed by Mandel and Salençon (1972) for homogeneous soils, and by Matar and Salençon (1977) for a case of shear strength increasing with depth [for an early attempt at the problem see Jürgenson (1934)]. The solutions were obtained by Mandel and Salençon and Matar and Salençon, using the slip-line method, assuming that the loaded boundary coincides with one of the slip lines. This is equivalent to an assumption that the shear stress along the loaded boundary is fully mobilized (inward-acting forces transmitted to the layer). Such assumption is quite realistic for the rigid footings for which these solutions were intended. While the resultant load on the foundation soil from embankments is vertical and equal to the weight of the fill, the outward-acting tangential load (with zero integral over the entire embankment width) is caused by the thrust in the embankment. Thus the characteristics of the load transmitted to the underlying soil are quite different for rigid footings and embankments [see also Jewell (1988)]. Nevertheless, it has been suggested that solutions by Mandel and Salençon (1972) and by Matar and Salençon (1977) be applied in design of embankments (Silvestri 1983; Bonaparte et al. 1987; Rowe and Soderman 1987). It should be emphasized that the solutions by Mandel and Salençon and by Matar and Salençon, were not intended by the authors to describe the bearing capacity under embankments, and the correctness of these solutions is not questioned here. Only the extension of their applicability to embankments is disputed.

It is proposed here that bearing capacity of layers loaded with an arbitrary horizontal component be calculated using the slip-line method. This method is shown to lead to the lower bound to the bearing capacity for layers resting

[1]Assoc. Prof., Dept. Civ. Engrg., Johns Hopkins Univ., Baltimore, MD 21218.
[2]Grad. Student, Dept. Civ. Engrg., Johns Hopkins Univ., Baltimore, MD.

Note. Discussion open until March 1, 1994. To extend the closing date one month, a written request must be filed with the ASCE Manager of Journals. The manuscript for this paper was submitted for review and possible publication on August 10, 1992. This paper is part of the ***Journal of Geotechnical Engineering***, Vol. 119, No. 10, October, 1993. ©ASCE, ISSN 0733-9410/93/0010-1657/$1.00 + $.15 per page. Paper No. 2284.

on perfectly rough bases. Only rough bases are considered here, which is the case most often appearing in practice (Humphrey and Holtz 1986). An upper-bound solution to the same problem (Michalowski 1993) is also used to indicate the range of possible deviation of the slip-line solution from the true limit load.

The slip-line solution to bearing capacity of a cohesive layer with strength increasing with depth is presented in the following section. Next, the upper-bound solution is presented and design charts are given. Also, calculations for a case history and a generic example of calculations of failure heights for reinforced and unreinforced embankments are given. Finally, some concluding remarks are presented.

SLIP-LINE SOLUTION

All considerations are restricted to plain-strain conditions because the length of the load from an embankment is considered large with respect to its width. The yield function of the cohesive soil is described by the Tresca condition (compression taken as positive)

$$F(\sigma_x, \sigma_z, \tau_{xz}) = \sqrt{(\sigma_x - \sigma_z)^2 + 4\tau_{xz}^2} - 2c = 0 \quad \ldots\ldots (1)$$

where c = shear strength of the soil (from an undrained test). Shear strength c is considered here to be a function of depth z

$$c = c_0 + \xi z \quad \ldots\ldots (2)$$

where c_0 = undrained shear strength at the top surface of the layer; and ξ = gradient of the strength with depth z. Differential equilibrium equations

$$\frac{\partial \sigma_x}{\partial x} + \frac{\partial \tau_{xz}}{\partial z} = 0 \quad \ldots\ldots (3a)$$

$$\frac{\partial \tau_{zx}}{\partial x} + \frac{\partial \sigma_z}{\partial z} = \gamma \quad \ldots\ldots (3b)$$

together with the yield condition in (1) lead to the following set of hyperbolic-type partial differential equations:

$$\frac{\partial p}{\partial x} - 2c \sin 2\psi \frac{\partial \psi}{\partial x} + 2c \cos 2\psi \frac{\partial \psi}{\partial z} = -\frac{\partial c}{\partial x} \cos 2\psi - \frac{\partial c}{\partial z} \sin 2\psi \quad \ldots\ldots (4a)$$

$$\frac{\partial p}{\partial z} + 2c \cos 2\psi \frac{\partial \psi}{\partial x} + 2c \sin 2\psi \frac{\partial \psi}{\partial z} = -\frac{\partial c}{\partial x} \sin 2\psi + \frac{\partial c}{\partial z} \cos 2\psi \quad \ldots\ldots (4b)$$

where ψ = angle of inclination of the major principal stress to the x-axis; and

$$p = \frac{\sigma_x + \sigma_z}{2} - \gamma z \quad \ldots\ldots (5)$$

γ = unit weight of the soil. This set of equations can be solved using the method of characteristics (slip-line method). The equations of the two families of characteristics (s_1 and s_2) are

$$\frac{dz}{dx} = \tan\left(\psi + \frac{\pi}{4}\right); \qquad s_1 \quad \ldots\ldots (6a)$$

$$\frac{dz}{dx} = \tan\left(\psi - \frac{\pi}{4}\right); \qquad s_2 \quad \ldots\ldots\ldots\ldots\ldots\ldots\ldots\ldots\ldots\ldots\ldots\ldots (6b)$$

and the relations along the lines expressed by (6) are

$$\frac{\partial p}{\partial s_1} + 2c\frac{\partial \psi}{\partial s_1} = -\frac{\partial c}{\partial x}\frac{\partial z}{\partial s_1} + \frac{\partial c}{\partial z}\frac{\partial x}{\partial s_1}; \qquad s_1 \quad \ldots\ldots\ldots\ldots\ldots\ldots\ldots\ldots\ldots\ldots (7a)$$

$$\frac{\partial p}{\partial s_2} - 2c\frac{\partial \psi}{\partial s_2} = \frac{\partial c}{\partial x}\frac{\partial z}{\partial s_2} - \frac{\partial c}{\partial z}\frac{\partial x}{\partial s_2}; \qquad s_2 \quad \ldots\ldots\ldots\ldots\ldots\ldots\ldots\ldots\ldots\ldots (7b)$$

For the type of nonhomogeneity considered here $\partial c/\partial x = 0$; and $\partial c/\partial z = \xi$. A solution to the stress problem using the slip-line method is then reduced to finding functions $p(x, z)$ and $\psi(x, z)$ satisfying the boundary conditions and (7) along the characteristics.

Two cases, an outward- and inward-acting horizontal load component on the layer, are considered separately.

Outward Horizontal Load on Layer

This is the simpler of the two cases. The field of the stress characteristics for a symmetrical half of a layer under an embankment of width $2b$ is shown in Fig. 1. The stress boundary conditions are as follows: (1) Zero traction along OA ($\psi = \pi$); (2) horizontal component of the stress vector on OP equal to $\bar{\tau} = \chi c_0[\psi = (\pi + \sin^{-1}\chi)/2$ on OP]; and (3) full mobilization of shear strength at CE ($\psi = 3\pi/4$ on CE). Coefficient χ representing the intensity of the horizontal load on the layer is defined as

$$\chi = \frac{\bar{\tau}}{c_0} \quad \ldots\ldots\ldots\ldots\ldots\ldots\ldots\ldots\ldots\ldots\ldots\ldots\ldots\ldots\ldots\ldots\ldots\ldots (8)$$

and is assumed positive for an outward-acting load, as in Fig. 1.

The solution requires solving (6) and (7) simultaneously, thus finding the slip-line network and functions p and ψ at every nodal point. The solution starts from boundary OA, and the Cauchy boundary value problem is solved in OAB (which happens to be the Rankine passive state). The jump in inclination of principal stress directions can easily be calculated at singular point O [$\Delta\psi = (\sin^{-1}\chi - \pi)/2$], and then the stresses can be found in region OBC by solving the degenerated characteristic problem. Next, a mixed problem is solved in OCD, where p and ψ are given along slip-line OC and ψ is given along boundary OD. Subsequently, two mixed problems are

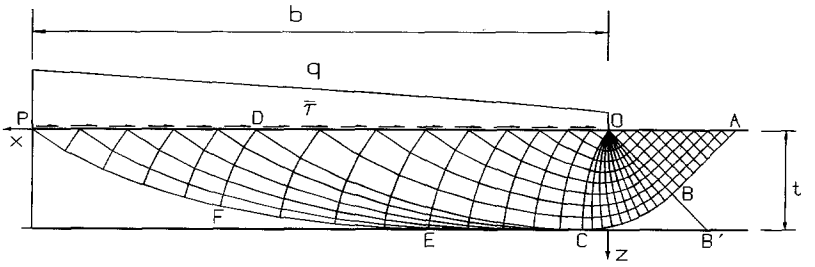

FIG. 1. Stress Characteristics Field in Layer Loaded with Outward Horizontal Component ($\chi = 0.25$; $\xi = 1.0$)

solved, in CDFE and in FDP. Because $\psi = 3\pi/4$ at CE, the characteristics of family s_1 are tangent to the base at CE (slip-lines s_2 approach CE at a right angle). Once function p is known at all nodal points along OP, the vertical components of the load causing the plastic state in the region marked by the characteristics can be calculated easily ($q = p + c_0\sqrt{1 - \chi^2}$). The shape of the distribution of limit load q for this particular example is marked in Fig. 1.

To prove that the total load on OP obtained is the lower bound to the true limit load, a statically admissible extension of the stress field needs to be found beyond the slip-line region. We assume here that the base-layer interface is rough (practical case), and the material below the base is rigid. Because point P is on the symmetry axis, it is a singular point with a jump in inclination of principal directions $\Delta\psi = -(\pi + \sin^{-1}\chi)/2$. Thus, a degenerated characteristic problem can be solved starting from point P and slip-line PFE, and, subsequently, a mixed boundary-value problem can be solved to reach the symmetry axis. The last two regions are then cut at the baseline, which does not violate the statical admissibility as long as the base interface is at least as strong as the soil (e.g., perfectly rough interface under compressive normal stress). Likewise, the admissible stress-field extension can be found beyond line ABC, where the Rankine state can be extended beyond line ABB′, and area CBB′ is part of the characteristic problem defined by lines BC and BB′.

Inward Horizontal Load on Layer

When the horizontal load on the layer points inward, the inclination of the major principal stress on OP drops below $\pi/2$ and a different solution is proposed beyond line ABCD (Fig. 2) to assure a continuous extension field. A mixed problem is solved in region EDJF (p and ψ given along ED, and ψ given along base EF), and another mixed problem in area DJHG (p and ψ given along DJ and ψ given along DG). In the latter, point G is found from the condition that characteristic GH must approach the symmetry axis at H at angle $\pi/4$ ($\psi = \pi/2$). It becomes clear now that the horizontal load component (or coefficient χ) cannot be specified along GP, because it would lead to an overconstrained problem in GHP. The mixed boundary problem in GHP is solved last (p and ψ are given along HG and $\psi = \pi/2$ on HP). The solution to this problem is then cut at GP and tractions along GP are calculated. Note that the horizontal load component at GP must drop from χc_0 at G to zero at P (symmetry axis). As in the previous case, the extension of the stress field can be found easily. Note that point H is not a singular

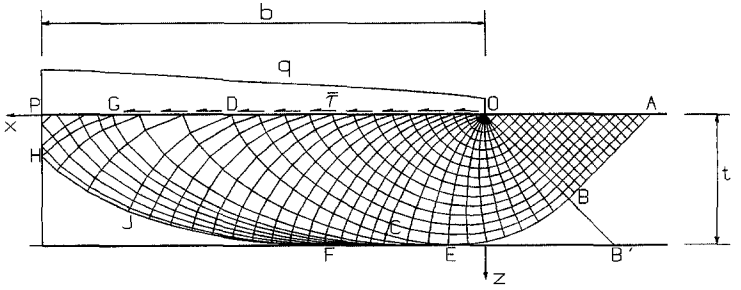

FIG. 2. Stress-Characteristics Field in Layer Loaded with Inward Horizontal Component ($\chi = -0.90$; $\xi = 1.0$)

point, and only one mixed boundary-value problem needs to be solved below line HJF (and cut along the base interface) to extend the slip-line field to the symmetry axis.

A particular solution to the bearing capacity of a layer, where $\chi = -1$, was given earlier by Mandel and Salençon (1972) for homogeneous soils, and by Matar and Salençon (1977) for a case in which the shear strength of the soil increases with depth. In this particular case the jump in inclination of principal directions at singular point O (Fig. 2) is $\Delta\psi = -3\pi/4$, so that last characteristic OC in fan OBC coincides with boundary OP, and all characteristics s_1 approach boundary OG at the right angle (s_2 tangent to OG).

UPPER-BOUND SOLUTION

The upper-bound approach of limit analysis is used here to indicate the possible deviation of the calculated limit loads from the true one. The soil is considered to be perfectly plastic and to conform to the flow rule associated with the Tresca yield condition. The upper-bound theorem states that in any kinematically admissible failure mechanism the rate of work done by tractions is less than or equal to energy dissipation. Thus, equating the rate of external work to internal dissipation in a kinematically admissible failure mechanism allows one to calculate the upper bound to the true limit load if the velocity of the loaded boundary is uniform.

The kinematically admissible mechanism of failure of a layer is shown in Fig. 3(*a*). The mechanism consists of rigid-motion blocks, except for area DEG, where a continual deformation occurs. The number of blocks in the mechanism changes, depending on ratio *b/t*. Kinematical admissibility requires that deformation be incompressible, thus all velocity jump vectors are tangent to their respective velocity discontinuities. Vertical velocity component V_0 is specified on boundary OBD. The respective velocities in the mechanism are presented on the hodograph in Fig. 3(*b*). Horizontal load $\bar{\tau} = \chi c_0$ is specified on OBD, while average vertical load $\bar{q}$ is the unknown. Note that since boundary OBD moves with a uniform vertical velocity component, the rate of work performed by q, and thus also the calculated average value $\bar{q}$, is independent of its actual distribution.

To preserve space, the details of the upper-bound solution are presented elsewhere (Michalowski 1993), although the results are shown in the next section along with the lower bounds. These results were obtained from

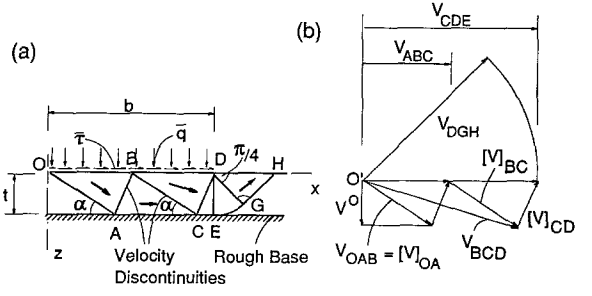

FIG. 3. (*a*) Collapse Mechanism of Layer for Upper-Bound Calculations; (*b*) Hodograph

calculations in which the minimum of $\bar{q}$ was sought, with angle α and the number of blocks in the failure mechanism [Fig. 3(*a*)] being variable.

COMPUTATIONAL RESULTS AND DESIGN CHARTS

Distributions of failure load q, resulting from the slip-line method, as functions of distance x from point O (edge of loading, Figs. 1 and 2) for different gradients of the soil strength ($\xi t/c_0$), are shown in Fig. 4. The distribution of q is shown for a horizontal load intensity represented by coefficient χ in the range of -1.0–0.8, in 0.2 intervals. Fig. 5 shows average vertical limit loads on layers under an embankment of width $2b$ as functions of dimensionless half-width (b/t). The solid lines are obtained through respective integration of the functions in Fig. 4, and the bullets come from the upper-bound approach. Both the lower- and upper-bound solutions are very close to each other (within a few percent) for low increase of soil strength with depth ($\xi t/c_0 \leq 1.0$), and the difference becomes close to 10% for $\xi t/c_0 = 2.0$.

The upper limit on χ ($\chi = 1.0$) is indicative of the surface failure. The

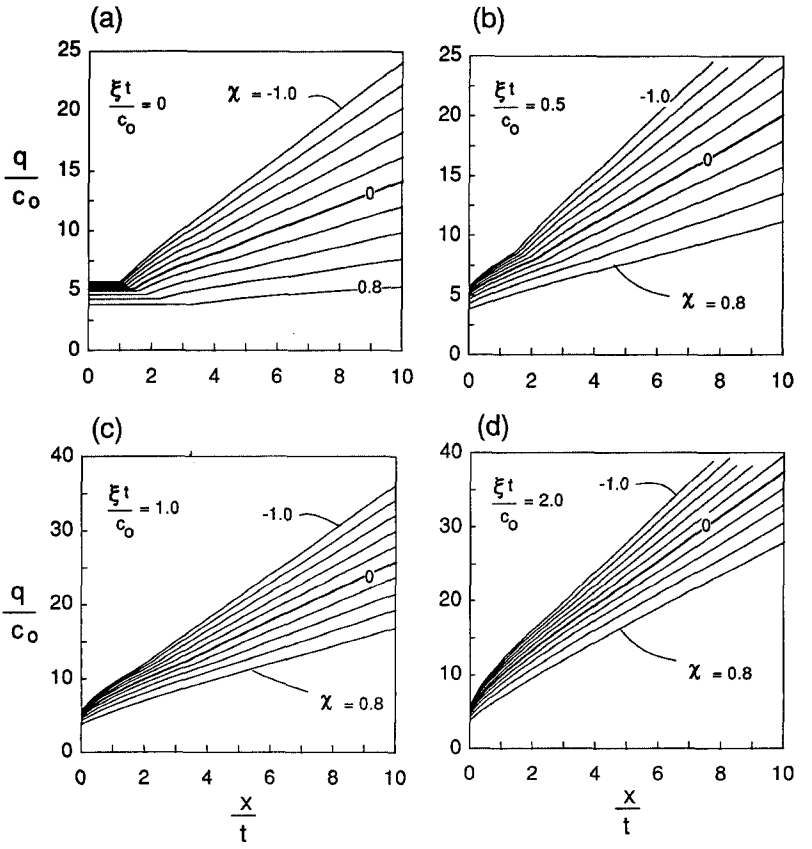

FIG. 4. Dimensionless Vertical Component of Limit Load q/c_0 as Function of Distance from Edge of Loading (Slip-Line Solution)

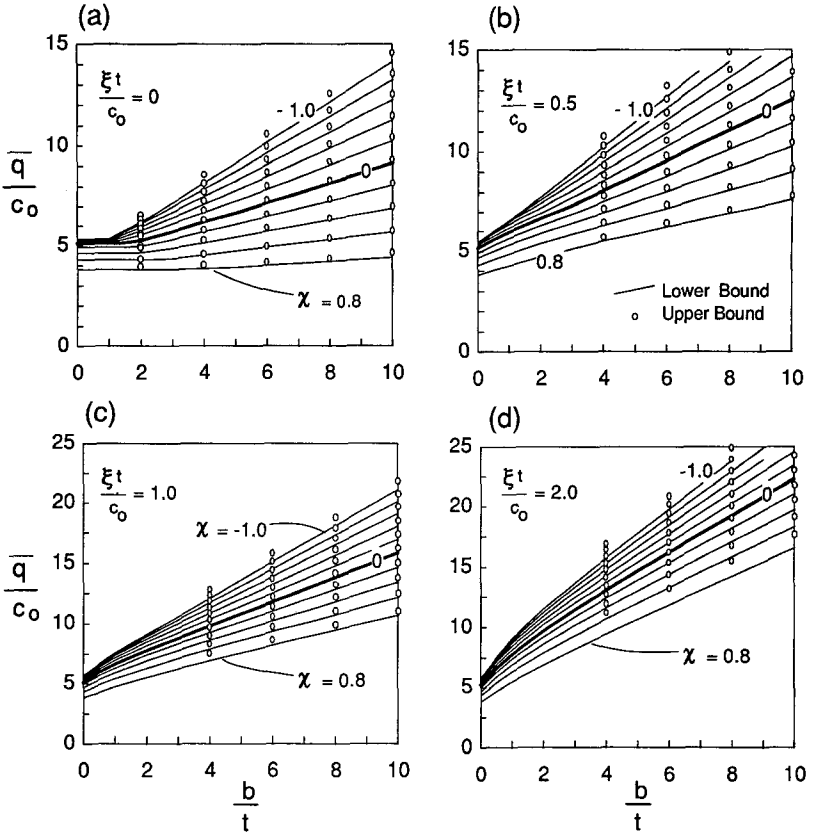

FIG. 5. Average Limit Load $\bar{q}/c_0$ as Function of Half-Width-to-Thickness Ratio

strength increase with depth then has no influence on the bearing capacity, and a spreading-type of embankment failure can be expected at $\bar{q}/c_0 = 2.57$ (Michalowski 1992).

It is suggested that the diagrams in Fig. 5 be used for design purposes. An illustration is presented in the following section.

APPLICATION OF CHARTS IN DESIGN OF EMBANKMENTS

The total thrust in the embankment at the symmetry plane can be estimated as $P_H = \gamma_f H^2 K/2$ (Fig. 6), where H is the embankment height, γ_f is the unit weight of the fill, and K is the lateral pressure coefficient. This horizontal thrust, reduced by the force in reinforcement (if present), is transmitted to the foundation soil under each symmetrical part of the embankment. Hence coefficient χ is

$$\chi = \frac{\bar{\tau}}{c_0} = \frac{\gamma_f H^2 K - 2R}{2bc_0} \quad \ldots\ldots\ldots\ldots\ldots\ldots\ldots\ldots\ldots\ldots\ldots\ldots\ldots\ldots\ldots\ldots\ldots\ldots (9)$$

where R = a force in reinforcement per unit length of embankment. It is assumed here that the reinforcement fails in the tensile mode (not pull-out).

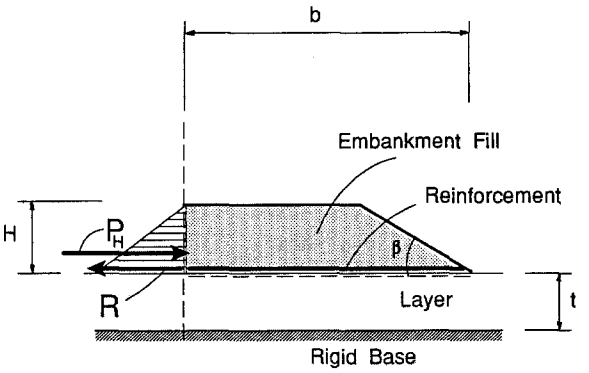

FIG. 6. Horizontal Forces in Embankment Fill

In limit-state analysis, R is equal to the tensile strength of reinforcement; for practical purposes R can be taken as a tensile force at some specified allowable lateral embankment strain. Coefficient K should not be smaller than $\tan^2(\pi/4 - \phi_f/2)$, with ϕ_f being the internal friction angle of embankment fill. For a conservative design, the coefficient of earth pressure at rest, $K = 1 - \sin \phi_f$, is recommended.

Theoretically, χ can vary from -1.0 to 1.0. If χ calculated from (9) reaches -1.0, the embankment is referred to as a fully reinforced embankment. An increase in the amount of reinforcement beyond that assuring $\chi = -1.0$ does not lead to an increase in failure height (or a factor of safety if the height is given). Under working conditions, coefficient χ is likely to be positive. Only at the onset of failure, when the soft soil begins to be "squeezed out" from underneath the embankment (incipient failure), may the total thrust in the embankment be equilibrated by the force in the reinforcement, and a further increase in the reinforcement force due to movement of the foundation soil with respect to the fill may cause inward horizontal forces (negative χ).

Although theoretically χ attains the value of -1.0 during failure of the foundation soil, a reasonable design criterion should not allow a value of χ much less than zero (zero for conservative design).

After χ is calculated from (9), Fig. 5 can be used to arrive at average limit pressure $\bar{q}$. The weight of the embankment $\gamma_f(2bH - H^2 \cot \beta)$ cannot exceed the total limit load $2\bar{q}b$; thus, the failure height is

$$H = b \tan \beta \left(1 - \sqrt{1 - \frac{2\bar{q}}{b\gamma_f \tan \beta}}\right) \quad \ldots\ldots\ldots\ldots\ldots\ldots\ldots\ldots\ldots\ldots (10)$$

where β = slope angle. Because χ is a function of H, the process of finding the critical embankment height is iterative. If $\bar{q}$ becomes large enough so that the function under the square root becomes negative, the embankment height becomes limited by its maximum value of $b \tan \beta$. Alternatively, as suggested in the literature (Bonaparte et al. 1987; Rowe and Soderman 1987), the computational width of the embankment can be taken at its midheight and the failure height can be calculated as $H = \bar{q}/\gamma_f$.

In the following, the failure heights for a known case history are calculated, accounting for an existing ditch in the foundation soil. Also, a generic

example of calculation of the failure height due to bearing capacity failure is presented.

Case History

A large number of case histories was assembled by Humphrey and Holtz (1986). Unfortunately, as noted by the authors, out of the 37 cases reviewed only a few have enough fairly well-documented data to be of any use in verification of design methods. In the following, critical heights of reinforced and unreinforced embankments are predicted for test embankments at Almere, The Netherlands, reported by Brakel et al. (1982). The geometry of the problem differs from that considered earlier in that there is a trench next to the embankment (see insert in diagram in Fig. 7). The thickness of the weak layer is taken as 3.75 m (a variable thickness of 3.0–4.5 m was reported), with a homogeneous undrained shear strength of $c = 8$ kN/m^2 and a specific weight $\gamma = 13$ kN/m^3 [from Fig. 10 in Brakel et al. (1982)]. The embankment half-width is $b = 8$ m [estimated from graphs in Brakel et al. (1982); the actual embankment was not symmetrical]; and the embankment fill was cohesive, with undrained shear strength probably about 5 kN/m^2 ("not fit to be walked on"), and $\gamma_f = 18$ kN/m^3. The fill inclination was about 35°. The trench was 2 m deep, its slope inclination was 35°, and it was offset from the embankment edge by about 0.7 m. This offset was neglected in calculations.

The calculations, using the upper bound technique, were modified to account for the trench slope, and the results are shown in Fig. 7 for $\chi = -1$ and $\chi = 0$; $\bar{q}/c$ is now dependent on the specific weight of the foundation soil (here $\gamma t/c = 6.1$). Note that the upper- and lower-bound solutions for a case without a trench were only a few percent apart [Fig. 5(*a*)], but adapting the upper-bound solution to account for the trench was considerably easier.

STABILENKA 200 was used as the reinforcement in the embankment, with a tensile strength of 200 kN/m (Ingold and Miller 1988). Due to its large tensile strength it is predicted that the force in reinforcement during bearing capacity failure will not reach its full strength, thus $\chi = -1$ (fully reinforced embankment). For $b/t = 8/3.75 \approx 2.13$ the value of $\bar{q}/c$ read from the diagram in Fig. 7 equals 4.6, and the failure height calculated from (10) becomes 2.69 m, only 2% below the reported height of 2.75 m, when

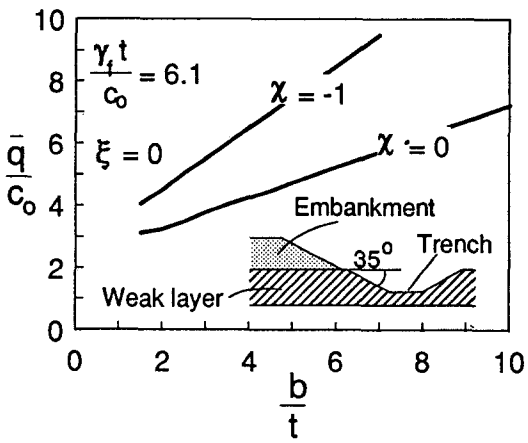

FIG. 7. Average Limit Load on Weak Layer with Trench (Upper Bound)

the excessive horizontal displacements in the embankment and the adjacent trench slope occurred. Horizontal thrust in the embankment with a cohesive backfill can be calculated as $P_H = \gamma_f(H - 2c_f/\gamma_f)^2/2$, with the assumption of the tensile crack to the depth of $2c_f/\gamma_f$. Utilizing relation $\chi = \bar{\tau}/c = (P_H - R)/cb = -1$ (see Fig. 6), the maximum force in the reinforcement during bearing-capacity failure is calculated: $R = 105$ kN/m. This is about 10% more than the 95 kN/m reported by Brakel et al. (1982) as measured some distance from the toe, but, as correctly predicted earlier, less than the tensile strength of the reinforcement. The tensile strength in the reinforcement was reached later, however, when the embankment slope was reported to have failed (at the same height) and the fabric was found to be torn.

In calculations of the failure height of the unreinforced embankment coefficient χ was assumed as zero, because no sufficient data for the fill was reported to calculate a reliable χ; $\bar{q}/c$ from Fig. 7 is now 3.3, and failure height from (10) becomes 1.74 m. This is almost exactly the same as the reported failure height of 1.75 m.

The failure heights calculated are surprisingly close to the ones reported by Brakel et al. (1982). It should be noted that the margin of error caused by the inaccuracies in determining the material parameters is far greater than the 2% suggested in the calculations. For instance, assuming that the shear strength of the foundation layer is determined with a reasonable level of confidence to be in the range of 7–9 kN/m^2 (rather than precisely 8 kN/m^2), the calculated failure heights for a fully reinforced embankment become 2.24–3.23 m (2.75 m ± 18%), and for an unreinforced embankment 1.48–2.01 m (1.75 m ± 15%).

Example

To present an application of the charts in Fig. 5 in predictions of failure heights of embankments, an example is shown here in which the layer's thickness is $t = 5$ m, undrained shear strength at the surface $c_0 = 5$ kN/m^2, and at the bottom of the layer $c = 10$ kN/m^2 ($\xi t/c_0 = 1.0$). The embankment fill is granular, $\gamma_f = 18$ kN/m^2, $\phi_f = 35°$. The half-width of the embankment $b = 20$ m, and the embankment slope is 1:2 ($\beta = 26.6°$). Failure heights will be calculated for three cases: without reinforcement, with reinforcement of tensile strength 50 kN/m, and for a fully reinforced embankment ($\chi = -1$). Note that since the intensity of the horizontal load on the layer depends on the embankment height [(9)], the process of finding the failure height is iterative. If the first guess of the height is too far from the actual failure height, the iteration process does not converge, and it was found out that guessing first coefficient χ is more practical, since the limits for χ are well defined.

For the case of no reinforcement, coefficient χ is positive, and a value of 0.20 is taken as a guess for the first iteration. The value of $\bar{q}/c_0$ is now read from Fig. 5(*c*) as 9.25, and the failure height is calculated from (10): $H = 3.03$ m. Now, the second iteration starts with calculations of χ from (9): $\chi = 0.22$ [$R = 0$; and $K' = \tan^2(\pi/4 - \phi_f/2)$]. Fig. 5(*c*) is used again to read $\bar{q}/c_0 = 9.1$. The new height from (10) is now 2.97 m. The value of χ from (9) for the third iteration is $\chi = 0.215 \approx 0.22$, which is equal to the value at the start of the second iteration. Hence, $H = 2.97$ m is the failure height of the unreinforced embankment.

The process of finding the failure height of the reinforced embankment is similar, but in (9) we now substitute $R = 50$ kN/m. If the thrust in the embankment is larger than the strength of reinforcement, χ will have a

positive value, otherwise $\chi \leq 0$. We assume the first guess as $\chi = 0$, thus $\bar{q}/c_0 = 9.8$ [Fig. 5(*c*)] and $H = 3.25$ m [(10)]. The next two iterations lead to $\chi = -0.24$; $\bar{q}/c_0 = 10.4$; $H = 3.50$ m; and $\chi = -0.20$; $\bar{q}/c_0 = 10.3$; $H = 3.46$, respectively; and $H = 3.46$ m is the failure height.

For a fully reinforced embankment $\chi = -1$, and calculation of the failure height is not iterative. From Fig. 5(*c*) $\bar{q}/c_0 = 12.1$, and the critical height of the fully reinforced embankment is $H = 4.27$ [(10)]. Eq. (9) can now be used to find the minimum reinforcement strength that assures that the embankment is fully reinforced. Substituting $\chi = -1$ and rearranging (9) leads to $R = 144.5$ kN/m. An increase of the reinforcement strength beyond $R = 144.5$ kN/m will produce no increase in the failure height.

FINAL REMARKS

Lower- and upper-bound solutions were presented for bearing capacity of cohesive layers over rigid rough bases. The results were shown for an arbitrary intensity of a horizontal load caused by embankment fill. For the particular case in which $\chi = -1$ (maximum possible inward acting forces), the lower-bound solution obtained by the method of characteristics is identical to that obtained by Mandel and Salençon (1972) for homogeneous layers, and to that given by Matar and Salençon (1977) for layers with strength increasing with depth.

The slip-line method provides the distribution of the limit load on the foundation layer. These distributions were used to arrive at average limit loads as functions of the embankment half-width. This average load (or the total load) was proven to be the lower bound to the true limit load. The upper-bound solution obtained was found to be only a few percent above the lower bound. Only for strength increasing significantly with depth ($\xi t/c_0 \geq 2.0$) were the two solutions more than 10% apart. The failure mechanism selected in the upper-bound approach can, therefore, be considered a good one. This is an important observation since the upper-bound approach may be more useful in some instances, because it is more adaptable to geometrical irregularities (for instance, it was adapted here to account for the influence of a trench in the weak layer).

The example included in the paper shows calculations of failure heights for reinforced and unreinforced embankments. A similar process can be adopted in design, with appropriate factors of safety. The thrust in the embankment was calculated assuming the active limit state in the embankment fill during failure. For design purposes it would be prudent to assume the lateral pressure coefficient [in (9)] as $K_o = 1 - \sin \phi$ rather than $K_o = \tan^2(\pi/4 - \phi_f/2)$. Also, for design purposes, coefficient χ should not drop much below zero (zero for a conservative design), since mobilization of the inward-acting forces requires a significant lateral deformation of the embankment. Finally, the force in the reinforcement taken in the examples as the reinforcement tensile strength should be estimated, for practical purposes, as the force in the reinforcement associated with a specified allowable deformation of the embankment.

The method proposed for calculations of embankment failure heights is simple, and may prove to be a useful design tool. It needs to be noted, however, that the bearing capacity type of failure is only one possible mode of embankment collapse, and the design process must also consider embankment slope failure and "spreading."

ACKNOWLEDGMENT

This research was sponsored by the National Science Foundation under grant MSS 9107778.

APPENDIX I. REFERENCES

Bonaparte, R., Holtz, R. D., and Giroud, J. P. (1987). "Soil reinforcement design using geotextiles." *Symp. on Geotextiles, Geomembranes and Related Products; STP 952*, J. E. Fluet, ed., ASTM, Philadelphia, Pa., 69–116.

Brakel, J., Coppens, M., Maagdenberg, A. C., and Risseeuw, P. (1982). "Stability of slopes constructed with polyester reinforcing fabric; test section at Almere, Holland '79." *2nd Int. Conf. on Geotextiles*, Industrial Fabrics Association Int., Las Vegas, Nev., Vol. III, 727–732.

Humphrey, D. N., and Holtz, R. D. (1986). "Reinforced embankments—a review of case histories." *Geotextiles and geomembranes*, 4, 129–144.

Ingold, T. S., and Miller, K. S. (1988). *Geotextiles handbook*. Thomas Telford, London, England.

Jewell, R. A. (1988). "The mechanics of reinforced embankments on soft soils." *Geotextiles and Geomembranes*, 7, 237–273.

Jürgenson, L. (1934). "The application of elasticity and plasticity to foundation problems." *J. Boston Soc. Civ. Engrg.*, 21, 206–241.

Mandel, J., and Salençon, J. (1972). "Force portante d'un sol une assise rigide (étude théorique)." *Géotechnique*, London, England, 22(1), 79–93.

Matar, M., and Salençon, J. (1977). "Capacité portante a une semelle filante sur sol purement cohérent d'épaisseur limitée et de cohésion variable avec la profondeur." *Annales de l'Institute Technique du Batiment et des Travaux Publics, Suplément No. 352, Serie: Sols et Fondations*, Paris, France, 143, 95–107 (in French).

Michalowski, R. L. (1992). "Bearing capacity of nonhomogeneous cohesive soils under embankments." *J. Geotech. Engrg.*, ASCE, 118(7), 1098–1118.

Michalowski, R. L. (1993). "Limit analysis of weak layers under embankments." *Soils and Found.*, 33(1), 155–168.

Rowe, R. K., and Soderman, K. L. (1987). "Stabilization of very soft soils using high strength geosynthetics: the role of finite element analyses." *Geotextiles and Geomembranes*, 6, 53–80.

Silvestri, V. (1983). "The bearing capacity of dikes and fills founded on soft soils of limited thickness." *Can. Geotech. J.*, 20, 428–436.

APPENDIX II. NOTATION

The following symbols are used in this paper:

b = half-width of embankment;
c = cohesion or undrained shear strength of foundation layer;
c_f = shear strength of cohesive embankment fill;
c_0 = shear strength at surface;
H = embankment height;
K = coefficient of lateral pressure;
P_H = horizontal thrust in embankment;
p = stress parameter, $p = (\sigma_x + \sigma_z)/2 - \gamma z$;
q = vertical limit pressure over foundation soil layer;
$\bar{q}$ = average vertical limit pressure over foundation soil layer;
R = tensile force in reinforcement per unit length of embankment;
t = layer thickness;
β = slope inclination angle of embankment;
γ = unit weight of foundation soil;

γ_f = unit weight of embankment fill;
ξ = strength gradient;
χ = horizontal load intensity, $\chi = \bar{\tau}/c_0$;
$\bar{\tau}$ = average shear stress on embankment fill–foundation soil interface;
ϕ_f = internal friction angle of embankment fill; and
ψ = angle of inclination of major principal stress direction to x-axis.